JACS
JOURNAL OF THE AMERICAN CHEMICAL SOCIETY

Article

pubs.acs.org/JACS

Sequence-Dependent Mechanism of DNA Oligonucleotide Dehybridization Resolved through Infrared Spectroscopy

Paul J. Sanstead,[†] Paul Stevenson,[†,‡] and Andrei Tokmakoff*[,†]

[†]Department of Chemistry, Institute for Biophysical Dynamics, and James Franck Institute, The University of Chicago, 929 East 57th Street, Chicago, Illinois 60637, United States

[‡]Department of Chemistry, Massachusetts Institute of Technology, 77 Massachusetts Avenue, Cambridge, Massachusetts 02139, United States

Supporting Information

ABSTRACT: Despite its important role in biology and nanotechnology, many questions remain regarding the molecular mechanism and dynamics by which oligonucleotides recognize and hybridize to their complementary sequence. The thermodynamics and kinetics of DNA oligonucleotide hybridization and dehybridization are often assumed to involve an all-or-nothing two-state dissociation pathway, but deviations from this behavior can be considerable even for short sequences. We introduce a new strategy to characterize the base-pair-specific thermal dissociation mechanism of DNA oligonucleotides through steady-state and time-resolved infrared spectroscopy. Experiments are interpreted with a lattice model to provide a structure-specific interpretation. This method is applied to a model set of self-complementary 10-base-pair sequences in which the placement of GC base pairs is varied in an otherwise AT strand. Through a combination of Fourier transform infrared and two-dimensional infrared spectroscopy, experiments reveal varying degrees of deviation from simple two-state behavior. As the temperature is increased, duplexes dissociate through a path in which the terminal bases fray, without any significant contribution from loop configurations. Transient temperature jump experiments reveal time scales of 70−100 ns for fraying and 10−30 μs for complete dissociation near the melting temperature. Whether or not frayed states are metastable intermediates or short-lived configurations during the full dissociation of the duplex is dictated by the nucleobase sequence.

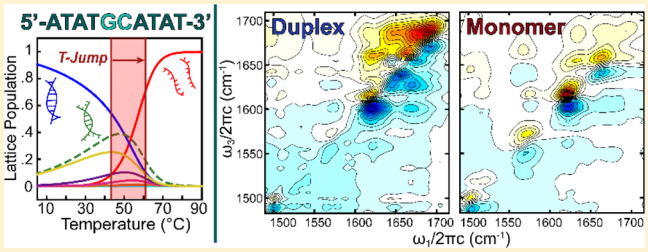

INTRODUCTION

The hybridization and dissociation of nucleic acids are central events in numerous biological processes ranging from replication[1,2] to gene regulation,[3,4] as well as technological applications ranging from bioassays[5,6] to DNA nanotechnology.[7,8] Technological applications depend on the remarkable property of high-fidelity base pairing that results in selective binding between complementary sequences and the growing predictive power in designing sequences for self-assembly. It is well established that many factors influence the thermodynamics and kinetics of DNA hybridization, including strand length,[9,10] strand concentration,[11,12] base composition,[13,14] and concentrations of monovalent and divalent cations.[15]

Even though our knowledge of the thermodynamics of DNA hybridization is broad, our understanding of the kinetics, dynamics, and molecular mechanism by which single-stranded oligonucleotides diffuse into contact, recognize, and hybridize to their complementary sequence remains limited. In addition to the atomistic insight provided by all-atom molecular dynamics simulations,[16−18] recently developed coarse-grained methods that represent DNA with a reduced number of interaction sites per nucleotide have simulated the hybridization mechanism in detail.[19,20] These models predict rich hybridization dynamics, including initial nucleation of a few key contacts followed by zippering of the remaining base pairs, shifted register slithering of one strand along another, and various internal displacement schemes depending on the nucleobase sequence.[21,22] At this time, additional experimental insight is required to directly investigate these or other potential mechanisms. Past studies relying on ultraviolet (UV) hyperchromicity lack base-specific structural sensitivity.[9,14,23] Förster resonance energy transfer experiments offer localized insight into strand proximity,[24−26] but they do not directly reveal pairing between individual bases, and they raise questions regarding how the fluorescent tag may potentially alter the dissociation mechanism.

The experimental challenges are such that we are still limited in our ability to characterize structural variation in DNA oligonucleotide duplexes. Especially for short sequences, DNA melting is often assumed to proceed in an all-or-nothing two-state fashion in which all of the base pairs are either entirely intact or broken, but in reality dimers have the potential to adopt a variety of partially associated states. The two-state assumption greatly simplifies the analysis and proves to be an adequate description for many applications involving both

Received: June 7, 2016
Published: August 12, 2016

DOI: 10.1021/jacs.6b05854
J. Am. Chem. Soc. 2016, 138, 11792−11801

oligonucleotide and polymeric DNA.[11,13,27] However, evidence suggests that deviations from the two-state assumption are possible for short sequences and even probable with certain motifs such as terminal AT base pairs, highly heterogeneous sequences, and hairpin structures.[28−33]

Experimentally, UV absorption spectroscopy is the most widely used method to track the thermal denaturation of DNA, where the hyperchromicity at ∼260 nm traces the melting curve. A van't Hoff analysis can be performed to extract the enthalpy, entropy, and free energy of dissociation, assuming that a two-state picture is adequate. Comparing calculated van't Hoff thermodynamics to model-independent calorimetric results is a common check for multistate behavior, where a discrepancy suggests a failing of the two-state model.[12,31] The standard UV method is rapid and convenient and requires a small amount of sample, but it offers little structural or mechanistic insight into dehybridization.

In order to describe DNA dehybridization in finer detail, a structurally sensitive experiment that can observe and quantify partially associated configurations of complementary strands on the time scale of their interconversion is desirable. For kinetic studies, the picosecond to millisecond time scales relevant to nucleic acid structural changes necessitate techniques with sufficient temporal resolution, which have included time-resolved infrared (IR),[34,35] UV,[9,14,23,31] and fluorescence spectroscopies.[25,36] The more complex challenge involves untangling stable thermodynamic intermediates with varying degrees of disorder from transiently formed kinetic states.

To address this challenge, we have developed an IR spectroscopy-based strategy to characterize the dehybridization of DNA oligonucleotides. The IR spectral region from 1450 to 1800 cm^{-1} contains in-plane base vibrations including carbonyl stretches and ring breathing modes that provide a unique fingerprint for each of the four DNA nucleobases.[37] Furthermore, the spectrum in this region is shaped dramatically depending on whether or not a base is paired or free.[38] Through a combination of Fourier transform infrared (FTIR) and two-dimensional infrared (2D IR) spectroscopy, the dehybridization of DNA strands can be tracked at a level of detail that distinguishes GC and AT base pairs. Equilibrium melting experiments are complemented with transient temperature jump (T-jump) experiments that track the nanosecond to microsecond dissociation dynamics of DNA oligonucleotides in real time. To provide a detailed interpretation of spectroscopic results, we use a lattice model that builds on the nearest-neighbor (NN) model[13] and allows the explicit consideration of partially melted duplex configurations. This model accurately captures the melting temperature (T_m) as well as the shape of the melting curve and provides an extra level of insight into the sub-populations of intact AT and GC base pairs for the sequences studied here. In this study, the method has been applied to a model set of self-complementary DNA 10-mers where the placement of GC base pairs is varied in an otherwise AT sequence. Pre-melting events such as fraying are distinguished from the loss of final contacts resulting in dissociation to the monomer state. We find that the propensity to fray as well as the manner in which fraying proceeds is dictated by the placement of the GC pairs within the sequence.

RESULTS

Temperature Ramp FTIR. For the purposes of developing the methods and analysis required to characterize the dissociation of DNA oligonucleotides using IR spectroscopy, we designed a set of model sequences that have the same length and base pair content, but varying base sequence. Since GC base pairs show greater stability than AT base pairs,[39] we expect that different regions of the oligomers will have contrasting thermodynamics, assuming they do not melt in a strictly two-state manner. Additionally, the placement of GC pairs in an otherwise AT sequence provides a natural and noninvasive probe of local structure. An oligonucleotide set that fits these criteria is 5′-ATATGCATAT-3′ (GC-core), 5′-ATGAT-ATCAT-3′ (GC-mix), 5′-GATATATATC-3′ (GC-ends), and 5′-ATATATATAT-3′ (AT-all). We will refer to the sequences by the shorthand names given in parentheses for convenience. We use the term "dimer" to represent any configuration of two associated strands, while "monomer" refers to a single strand without hydrogen bonds to another strand.

As an initial assessment, FTIR temperature ramp experiments were performed to track the helix-to-coil transition between 5 and 90 °C. We have previously assigned the vibrational modes for each of the nucleobases in the 1500−1700 cm^{-1} range, finding these vibrations to be highly coupled and delocalized across the base.[37] In the thermally dissociated state, the IR spectrum closely resembles a composition-weighted sum of the individual free nucleotides that make up the sequence, but variations between the sequences, primarily small differences in ring mode intensity, reflect differing degrees of single strand stacking interactions in the monomer. In contrast, the formation of a DNA duplex significantly influences and shapes the vibrational frequencies, intensities, and line shapes.[38,40] In addition, much of the character from the isolated bases is evident in the spectrum, allowing meaningful and base-specific structural insight. Many changes to the spectrum are apparent with increasing temperature (Figure 1), but the most prominent feature is the doubling in intensity of the 1622 cm^{-1} A ring mode upon duplex melting. This peak reports primarily on the amount of paired A since the intensity is suppressed upon the formation of a stacked and hydrogen-bonded Watson−Crick (WC) pair. Similar to the A ring mode, the C ring modes at 1503 and 1520 cm^{-1} as well as the G ring modes

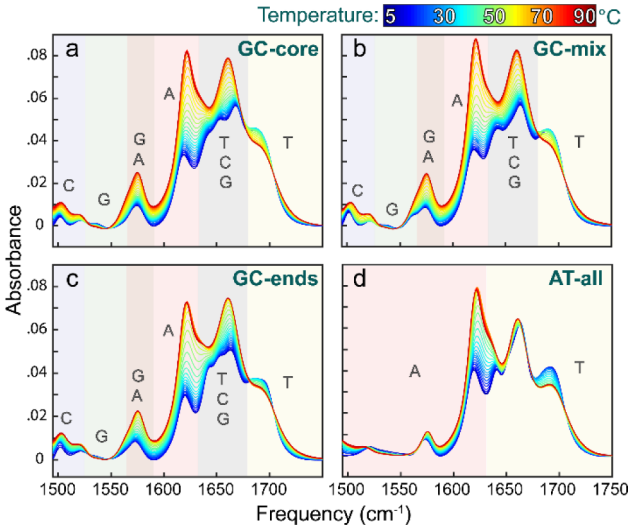

Figure 1. Temperature ramp FTIR spectra from 5 to 90 °C with 2 mM oligonucleotide, 50 mM pD 7.2 sodium phosphate buffer, 240 mM NaCl, and 18 mM $MgCl_2$ for (a) GC-core, (b) GC-mix, (c) GC-ends, and (d) AT-all. Shading indicates the contributions of the four nucleobases to the spectra.

DOI: 10.1021/jacs.6b05854
J. Am. Chem. Soc. 2016, 138, 11792−11801

at 1564 and 1575 cm^{-1} are likewise suppressed upon duplex formation. These features report on the status of GC base pairs, although the presence of an additional A ring mode at 1574 cm^{-1} (Figure 1d) that overlaps with the higher frequency G ring modes complicates things slightly. The shading in Figure 1 highlights the contributions from each of the nucleobases across the 1500−1750 cm^{-1} frequency range.

Above 1630 cm^{-1} the spectrum becomes congested, with multiple overlapping peaks. However, some base-specific information is still discernible, such as the T carbonyl mode at 1690 cm^{-1} that increases in intensity when T is paired. With increasing temperature, the loss of fine structure and the large intensity growth around 1660 cm^{-1} are due to increasingly unpaired T, C, and G, but the GC features in this frequency range are largely obscured beneath T contributions since the sequences have only 20% GC content.

Melting Curve Analysis. To describe the global spectral changes between 1495 and 1750 cm^{-1} upon dehybridization, we analyzed the IR spectra over the 5−90 °C temperature range using singular value decomposition (SVD). Temperature-dependent changes to the IR spectrum are obtained from the normalized second SVD component, shown in Figure 2 as the blue data points. Melting curves are obtained from these data by subtracting the sloping baselines, indicated by the dashed lines in Figure 2, at high and low temperature. In practice, the melting curves (Figure 3a) were extracted from a fit to a two-state thermodynamic model that allows for a temperature-dependent enthalpy and entropy, which is described by eq 4 in the Supporting Information (SI). Analyzing the full IR spectrum results in melting curves similar to those obtained by tracking the intensity of a single broad feature in the UV spectrum and therefore serves as the starting point of our analysis. We have previously compared the T_m trends obtained from FTIR and UV methods for DNA oligonucleotides, finding good agreement between the methods and with UV-based model predictions.[15,41] The melting curves are assumed to report on the fraction of intact base pairs (θ_{bp}), and T_m is defined as the temperature at which 50% of all base pairs are intact.[11,12]

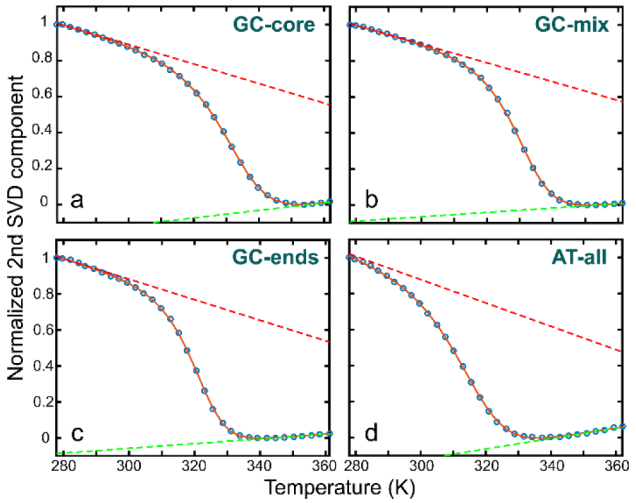

Figure 2. Normalized second SVD component from temperature ramp FTIR (blue points) fit to the two-state model described by eq 4 in the SI (solid red line). Sloping baseline fits are plotted for illustration using dashed lines.

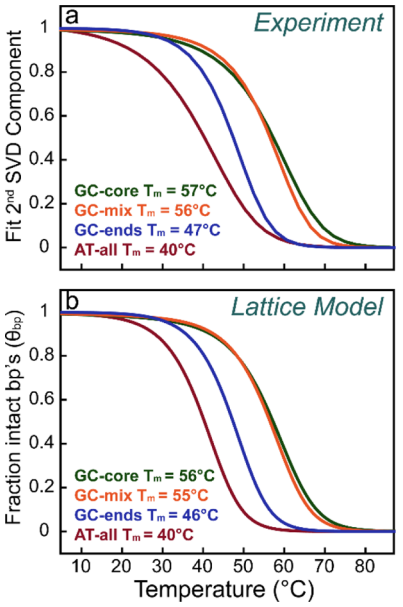

Figure 3. Comparison of melting curves (a) determined from a two-state analysis fit to the second SVD component from FTIR temperature ramps and (b) calculated from the fraction of intact base pairs in the lattice model.

It is apparent that the base sequence and composition determine both the shape of the melting curve and the melting temperature. AT-all, lacking any GC content, has the lowest T_m, at 40 °C. Despite their identical GC content, GC-core, GC-mix, and GC-ends show distinct melting curves due to the variable placement of the GC pairs in each sequence. The T_m for GC-ends is 47 °C, and the melting curve is a sharp sigmoid symmetric about the inflection point, as expected for two-state melting.[42] At 57 and 56 °C, both GC-core and GC-mix have a T_m that is shifted to higher temperature, but the shapes of the melting curves differ. Qualitatively, the four curves also vary in their slopes at $\theta_{bp} = 0.5$ as well as the degree of symmetry about that point. For example, slight deviation from a classic sigmoidal melting curve in the case of GC-core hints at a possible departure from two-state behavior; however, additional information is required in order to understand the sequence effects on dehybridization in detail. A comparison of classic van't Hoff analysis against fitting to a two-state model with a nonzero ΔC_P is included in the SI (Figure S2) as well as a comparison to the lattice model described below. We find that the agreement between the three thermodynamic descriptions is best for those sequences which most closely follow a two-state dissociation and that, in general, the model predictions are most consistent near T_m.

Temperature Ramp 2D IR. Despite the ability to clearly distinguish base-specific features in the FTIR, spectral congestion and overlap can pose a challenge when interpreting the spectra. As a step toward experimentally characterizing which bases are intact in partially melted dimer structures, we used 2D IR spectroscopy to report on base pairing of a single type, either AT or GC. 2D IR separates AT and GC reporter regions by spreading information out onto a second frequency axis. The peaks in a 2D IR spectrum consist of oppositely signed doublets (red above blue) with the on-diagonal peaks, mirroring the peaks in the linear spectrum and the off-diagonal cross peaks reporting on the coupling between the vibrational modes. In addition to the intensity changes and frequency shifts

DOI: 10.1021/jacs.6b05854
J. Am. Chem. Soc. 2016, 138, 11792−11801

discussed above, the formation of a WC pair gives rise to additional intermolecular cross peaks due to vibrational couplings across the hydrogen-bonded bases. These cross peaks offer a direct measure of the extent of intact WC pairs, and therefore tracking these off-diagonal features provides a means of isolating the response from either the AT or GC base pairs. Temperature ramp 2D IR was used to monitor the helix-to-coil transition for each of the sequences. Three representative 2D IR spectra from the GC-core temperature ramp (Figure 4) demonstrate the substantial spectral changes observed as the duplex melts and dissociates. The complete temperature ramp series is included in the SI (Figure S4).

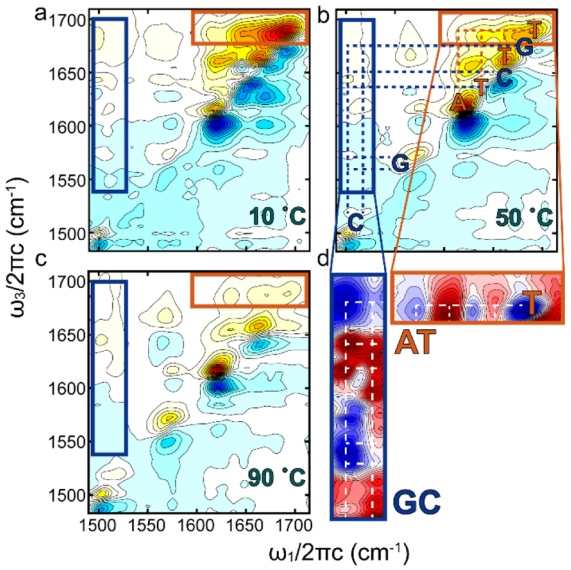

Figure 4. Representative 2D IR spectra at (a) 10, (b) 50, and (c) 90 °C from the GC-core temperature ramp. The GC and AT cross peak regions are indicated by the blue and orange boxes, respectively. Dashed lines serve as a guide for locating cross peaks. (d) The second SVD component spectra demonstrate the changes in the cross peak regions upon thermal dehybridization, with blue/red (red/blue) doublets representing loss (gain).

To separately quantify GC and AT base pairing, SVD analysis was performed on GC- and AT-specific cross peak regions. The blue box in Figure 4 defines the GC region and includes cross peaks between the 1500−1520 cm^{-1} C ring modes and the G ring modes in the 1540−1575 cm^{-1} range as well as the G carbonyl mode at 1680 cm^{-1}. The orange box defines the AT region and contains the 1690 cm^{-1} T carbonyl peak as well as its cross peaks to the lower frequency T modes and the 1625 cm^{-1} A ring mode. Dashed lines in Figure 4 illustrate the coupling of these features, while the second SVD component spectra (Figure 4d) demonstrate how these cross peaks change in response to duplex melting. A red above blue doublet represents intensity gain, while a blue above red doublet represents intensity loss. However, these cross peak regions are crowded with information, and many of the features overlap. As a result, much of the doublet structure is obscured; roughly, blue features represent intensity loss while red features represent intensity gain. The loss of intermolecular cross peaks is clearly visible as well as the gain of intramolecular cross peaks upon duplex dissociation as the vibrations are localized onto the unpaired base. Considering these regions independently, an effective melting curve for the AT (θ_{AT}) and GC (θ_{GC}) base pairs can be determined (Figure 5a−d) from the second SVD component, which reports on the temperature-dependent spectral changes. Additional results and discussion of the SVD analysis for all sequences are included in the SI (Figures S5 and S6).

Maximum Entropy Method To Reconstruct Spectral Component Amplitudes. To account for the possibility of spectroscopically resolvable structural heterogeneity in the dimer ensemble along the helix-to-coil transition, we employed a maximum entropy method to evaluate the minimum number of spectral components contributing to the temperature ramp FTIRs for each sequence.[43] The method is described in more detail in the SI. The reconstructed amplitudes are plotted in Figure 5e−h. All of the sequences have a spectral component that dominates at low temperature (blue) and a second that dominates at high temperature (red), suggesting these components correspond to the fully paired dimer and monomer, respectively. The third component amplitude (green) is therefore assigned as a spectral contribution from partially melted dimers.

The reconstruction for GC-core suggests a sizeable partially melted population along the helix-to-coil transition represented by the considerable third component amplitude, peaking at

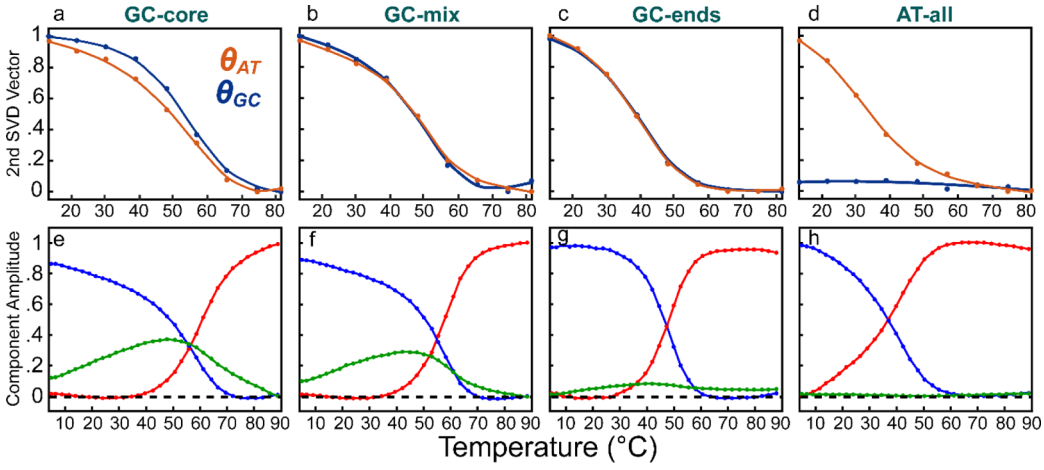

Figure 5. AT and GC melting curves measured from temperature ramp 2D IR (top panel) and the maximum entropy reconstructed spectral amplitude profiles from the FTIR SVD analysis (bottom panel) for (a,e) GC-core, (b,f) GC-mix, (c,g) GC-ends, and (d,h) AT-all.

DOI: 10.1021/jacs.6b05854
J. Am. Chem. Soc. 2016, 138, 11792−11801

nearly 40%, ~10 °C below T_m. Insight from 2D IR reveals the nature of these partially melted configurations. The θ_{GC} transition is shifted to higher temperatures with respect to θ_{AT} and appears to be a sharper, more two-state-like transition, while θ_{AT} appears to have a more gradual and sloped upper baseline, indicating loss of AT contacts at temperatures well below T_m (Figure 5a). These results suggest a dissociation pathway where the terminal AT base pairs begin to fray, yielding an ensemble of fully duplexed and partially melted dimers. However, from the perspective of a GC base pair embedded within the core of the sequence, dissociation is essentially two-state, consistent with the sharper transition observed for θ_{GC}. GC-mix shows a less pronounced contrast between θ_{GC} and θ_{AT} as well as a smaller contribution from a third spectral component amplitude, consistent with a reduced population of partially melted dimers with respect to the GC-core (Figure 5b). The maximum entropy third component amplitude is virtually flat, and the AT/GC base pair fractions from 2D IR are essentially overlaid for GC-ends (Figure 5c,g), as one would expect for two-state dissociation.

Temperature Jump Dissociation Kinetics. We tracked changes in the IR spectrum in response to a 5 ns, 18 °C T-jump to provide a direct window into the dehybridization mechanism. The T-jump spectrometer and experiment have been described in detail previously.[44,45] Instead of collecting T-jump difference spectra for the full 2D IR surface, we collected transient heterodyned dispersed vibrational echo (t-HDVE) spectra, which are related to the projection of the 2D IR spectrum onto the ω_3 axis. Since the ω_1 axis is not resolved, the data acquisition time is significantly faster, allowing finer sampling of kinetic traces. However, projection onto a single frequency axis can result in overlapping spectral features that must be accounted for when interpreting t-HDVE data. The spectral changes in the temperature ramp 2D IR spectra (Figure 4) serve as a valuable guide when identifying features that track the GC and AT responses independently. The induced absorption of the A ring mode centered around 1595 cm^{-1} demonstrates substantial intensity change upon loss of AT pairing and, when projected onto the ω_3 axis, provides a clear marker for the AT features. Similarly, the response of the induced absorption of the G ring modes centered around 1545 cm^{-1} serves as a reporter of GC base pairing.

Temperature jumps of 18 °C were performed across the center of the reconstructed spectral amplitude distributions, with the initial temperature set 5 °C below the maximum of the third component amplitude, plotted in green (Figure 5). Transient HDVE spectra for each of the sequences (Figure 6) reveal significant spectral changes in the time window from 5 ns to 100 μs. To distinguish changes specific to AT and GC pairs, the kinetics were tracked at 1595 and 1545 cm^{-1}, respectively. All transient responses rise away from the baseline until a T-jump delay of ~100 μs, after which the signal drops as a result of the temperature re-equilibration of the sample. The clear differences in the AT and GC kinetics in the case of the GC-core and GC-mix sequences illustrate the nucleobase specificity of these experiments. Whereas all of the equilibrium melting curves can be evaluated in terms of approximate two-state melting (SI), the T-jump experiments for three out of the four oligonucleotides show clear bimodal melting kinetics, which is inconsistent with the expectation for two-state unfolding, where all of the base pairs break in concert and one would expect a single consistent exponential trace, regardless of which base feature is tracked.

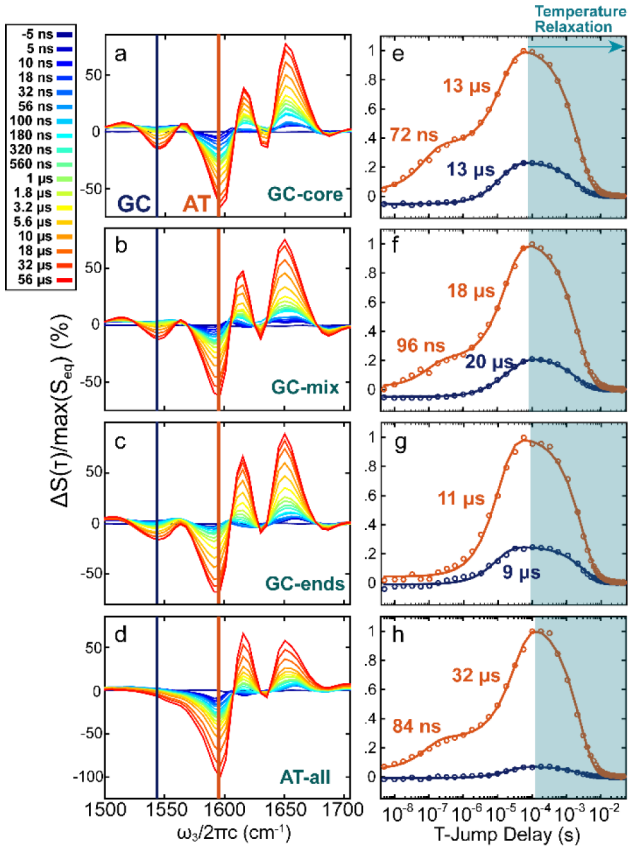

Figure 6. Transient HDVE spectra for the (a) GC-core, (b) GC-mix, (c) GC-ends, and (d) AT-all sequences. Kinetic traces tracked at the 1595 cm^{-1} AT (orange) and 1545 cm^{-1} GC (blue) frequencies normalized to the maximum of the AT trace. Displayed time constants are from exponential fits.

Fitting kinetic traces to exponentials to extract time constants, we find that both AT and GC traces for all of the sequences display a relaxation response between 10 and 30 μs, except the 1545 cm^{-1} trace for the AT-all sequence, which is essentially flat since there are no GC pairs in the sequence. This relaxation process is consistent with full dissociation into the monomer state since it is universal and concerted between the AT and GC base pairs.

A faster 70−100 ns response is observed only from the AT features for all of the sequences that have terminal AT pairs, but not for GC-ends, suggesting that the more weakly paired AT pairs at the termini respond more-or-less independently of the GC pairs more central to the helix. Therefore, this early time response would appear to involve fraying of the terminal AT base pairs. The magnitude of the fraying response is greatest for GC-core, consistent with a larger population of partially melted dimer configurations for this sequence, whereas GC-mix and AT-all show a reduced early time response. For GC-ends, both the AT and GC traces are well fit by a single-exponential rise, with a ~10 μs time constant consistent with a two-state dissociation mechanism. These observed time scales are in agreement with those reported previously for the unfolding and dissociation of small nucleic acid systems initiated by a rapid T-jump.[14,35]

Comparison to the Lattice Model. To help interpret experimental results in terms of conformational variation within the melting duplex ensemble, we used a statistical lattice model for DNA hybridization similar to those used by others,[23,46,47]

DOI: 10.1021/jacs.6b05854
J. Am. Chem. Soc. 2016, 138, 11792−11801

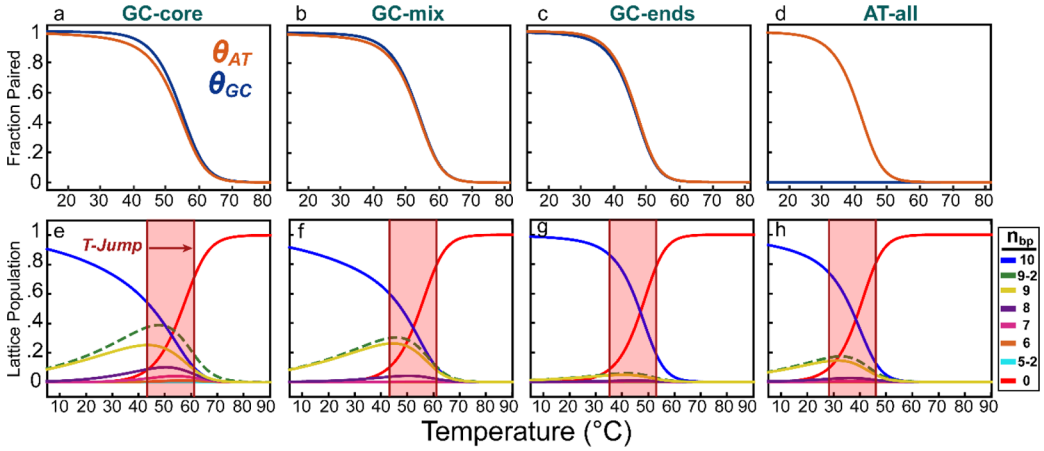

Figure 7. Lattice model AT and GC base pair fractions (a–d) and population profiles (e–h) for (a,e) GC-core, (b,f) GC-mix, (c,g) GC-ends, and (d,h) AT-all. The population curves correspond to fully intact dimers (blue), frayed dimers (dashed green), and fully dissociated monomers (red). Otherwise the microstates are grouped according to their number of intact base pairs, n_{bp}. The red shading indicates the temperature jumps from the t-HDVE experiments.

which we summarize here and discuss in more detail in the SI. The model enumerates the microstates available to complementary DNA strands, broadly grouping them according to their configuration of intact base pairs. The base pairing scheme for a particular microstate is represented by a 1D lattice of intact and broken base pair sites. The oligonucleotide conformation is reduced to a beaded chain, and the configurational degrees of freedom for unpaired bases are enumerated through self-avoiding random walks on a 3D cubic lattice. These base pair configurations range from fully and partially melted "dimer" microstates to fully dissociated "monomer" configurations. The statistical weight for a given configuration is assigned with a microstate enthalpy using the unified set of NN parameters developed by SantaLucia.[13] Additionally, translational degrees of freedom and concentration effects are generated through a separate 3D lattice where the formation of a dimer is defined by two molecules being adjacent on the lattice. For the purpose of comparing the lattice model to two-state thermodynamics, we calculate the dissociation constant for the dimer–monomer equilibrium, K_d, from monomer (fully dissociated strands) and dimer (all other configurations) partition functions in the SI.

The lattice model provides a detailed description of the temperature-dependent conformational variation within the ensemble of paired oligonucleotides. To demonstrate the model's predictions, Figure 7e–h illustrates the relative populations of conformers grouped by number of intact base pairs (n_{bp}) for each of the sequences. We observe that the fully base paired dimer and monomer account for the vast majority of the population at the temperature extremes. For both GC-core and GC-mix near T_m, a significant fraction of the population exists as conformers with only 6–9 intact base pairs, but conformers with <6 intact base pairs (n_{bp} = 2–5) have negligibly low populations. In the case of GC-mix, 99% of the total dimer population with one or more broken base pairs can be accounted for by states with only 1–2 broken base pairs, while for GC-core, 99% of the partially melted population can be accounted for by states with only 1–4 broken base pairs. Within these disordered configurations, those with frayed ends are heavily favored over loop microstates, and we therefore call configurations with at least one broken and one intact base pair "frayed dimers", represented by the dashed green profiles in Figure 7e–h. To better visualize the composition of the n_{bp} sub-ensembles, contact plots that explicitly show the microstates and their associated populations are included in the SI (Figure S7).

The model predicts that, regardless of sequence, fraying initiates at the end of the helix, but how the accumulation of frayed dimer population proceeds as the temperature increases is dictated by the nucleobase sequence. GC-core frays more-or-less symmetrically around a stable core of intact base pairs, while GC-ends preferentially frays from one end of the helix. GC-mix and AT-all fray more asymmetrically than GC-core, but still from both ends of the helix. A common trend is a bias toward the preservation of intact GC over AT base pairs. Therefore, the placement of GC pairs within the sequence directs which configurations are populated along the helix-to-coil transition.

Furthermore, the lattice model provides a window into the starting ensemble for T-jump experiments and offers a sense of how the population will shift in response to the temperature change. The temperature ranges corresponding to the T-jump experiments above are indicated by the red shading in Figure 7. From the shifts in population, the model suggests that the majority of the nanosecond fraying response observed for GC-mix corresponds to the loss of a single terminal AT base pair. For GC-core, more diverse configurations are possible, with populated microstates tolerating up to four broken base pairs, but here still, much of the nanosecond response is likely accounted for by the loss of a single AT base pair.

To make more direct connections with experiment, the lattice model was used to calculate the average fraction of intact base pairs (θ_{bp}) for comparison against the FTIR melting curves for each of the sequences (Figure 3), as well as the fraction of intact AT (θ_{AT}) and GC (θ_{GC}) base pairs across the transition (Figure 7a–d) for comparison against the AT and GC melting curves determined by 2D IR (Figure 5a–d). The variation in melting temperatures as well as the shape of the melting curves calculated from the model agrees well with experiment. However, the agreement for the AT-all sequence is comparatively weak, with the experimental melting transition appearing less sharp than the model prediction. We believe this discrepancy arises from a combination of factors. The comparatively low T_m of 40 °C makes it difficult to accurately

DOI: 10.1021/jacs.6b05854
J. Am. Chem. Soc. 2016, 138, 11792–11801

subtract baselines from the melting curve (Figure 2). In addition, the repetitive AT-all sequence could have a significant contribution from overhanging shifted-registry states, which are currently not considered in the model.

It is interesting to note that θ_{GC} drops at a slightly lower temperature than θ_{AT} for GC-ends, in contrast to the GC-core/GC-mix sequences, where AT pairs are lost before GC. This result suggests that the GC base pairs at the end of the helix break at slightly lower temperatures than the AT core of the sequence, but that once the capping GC pairs go, the rest of the duplex easily follows. This description is consistent with those states predicted by the model to be appreciably populated for GC-ends as the temperature increases (SI, Figure S7).

With regard to the spectral component amplitudes reconstructed from FTIR (Figure 5e–h), we noted a strong resemblance of the third component amplitude, plotted in green, with the temperature-dependent populations of frayed dimers in the lattice model. In Figure 7e–h, we illustrate the lattice model population profiles grouped into three fractions: dimers with all base pairs intact (n_{bp} = 10, blue), frayed dimers where the populations of dimers with at least one broken and one intact base pair are summed together (n_{bp} = 2–9, dashed green), and monomer configurations lacking any intact base pairs (n_{bp} = 0, red). The similarity between the experimental spectral component amplitudes and the model predictions represented in this way is striking. It suggests that FTIR experiments are indeed sensitive to the heterogeneity of partially melted configurations in the dimer ensemble and that the population distributions of the lattice model are realistic.

It is important to note that the number of experimentally resolvable spectral components in equilibrium experiments does not necessarily correspond to the number of distinct thermodynamic states. Since the changes in the IR spectrum primarily reflect the number of intact vs broken base pairs at a given temperature, and the spectra at the temperature extremes provide limits on the true duplex vs the monomer spectrum, one would expect a resolvable spectral component between these extremes, if it exists, to correspond to those configurations which have at least some broken and some intact base pairs. The inability to resolve frayed dimers for AT-all (Figure 5h) despite the prediction of ~17% partially melted population near T_m is likely explained by the fact that the spectrum for this sequence (Figure 1d), having the most homogeneous composition, contains lower information content compared to the mixed AT/GC sequences, making it difficult to resolve a distinct third spectroscopic component using the maximum entropy method.

DISCUSSION

Our results indicate that IR spectroscopy can spectrally isolate different contacts within the DNA duplex, thereby giving base-pair-resolved information on melting transitions, conformational disorder, and melting kinetics. Using the AT and GC fractions measured from 2D IR spectroscopy in conjunction with the maximum entropy spectral component amplitudes, it is possible to experimentally resolve the heterogeneity of configurations in the dimer ensemble and to identify which base pairs are involved in the formation of frayed dimers. T-jump experiments reveal the kinetics involved in transitioning from a fully paired dimer through partially melted configurations into the random coil state.

Although the dynamics of dissociation vary with sequence, our results indicate that dissociation proceeds from the end of the helix for all of the sequences tested. This suggests a common dissociation pathway in which the terminal bases fray first, but where the stability of the resulting frayed configuration is dictated by the nucleobase sequence. Experimentally resolving the base-specific details of GC-ends dehybridization proves more challenging due to its effectively all-or-nothing behavior, and the evidence for terminal GC fraying should be regarded as suggestive rather than conclusive. However, in addition to the predicted offset between the θ_{AT}/θ_{GC} curves and the model prediction of a small frayed population consisting almost entirely of structures with a single broken terminal GC pair, it is worth noting the small deviation in the GC-ends 1545 cm^{-1} kinetic trace that peaks around 100 ns, visible in Figure 6g and highlighted in Figure S8 in the SI. Although the amplitude of this feature is too small to justify fitting a biexponential, the slight deviation from a single-exponential rise and the 2 μs shift in the GC time constant toward earlier time with respect to the AT time constant are both consistent with the presence of a small-amplitude nanosecond response, corresponding to a minor amount of GC fraying for this sequence. As a result of the low magnitude of this early time signal, we conclude that the GC-ends sequence represents an essentially classic two-state dissociation, but that dissociation still likely proceeds from the ends of the duplex in a mechanism consistent with the other sequences.

In addition to the T-jump evidence, the IR spectrum is significantly shaped depending on whether a base is WC paired or free in solution, and we would expect bubbling base pairs to be just as evident in the steady-state experimental data as fraying base pairs. However, we see no evidence for conformations in which internal AT base pairs bubble between intact capping GC pairs, suggesting a lower limit exists for the size of possible loop states and explaining why GC-ends dissociates in an apparent two-state manner. This lack of bubbling for DNA 10-mers is consistent not only with our own lattice model predictions but also with previous calculations that suggest bubbling is unfavorable for short oligonucleotides,[48,49] as well as experimental evidence suggesting a minimum length of ~20 base pairs is necessary to nucleate bubble formation.[50] Due to the previously discussed uncertainty regarding AT-all's melting curve and the fact that we are unable to resolve a third spectroscopic component from the FTIR maximum entropy reconstruction we cannot confidently analyze this sequence in detail at this time, but some degree of deviation from a simple two-state dissociation appears likely in light of our results. We propose, in order of increasing deviation from two-state behavior: GC-ends < AT-all < GC-mix < GC-core.

The lattice model allows direct consideration of the microstates populated along the helix-to-coil transition and can help inform the interpretation of the spectroscopic results. For GC-ends there is a lack of partially melted configurations, and the population is dominated by a ratio of completely intact duplex to monomer across the entire temperature range, as would be expected for a two-state dissociation (Figure 7g). For both GC-core and GC-mix, a sizeable frayed population is observed, with a nearly 40% and 30% contribution near T_m, respectively (Figure 7e–f). These stable partially melted configurations are characterized by the loss of terminal AT base pairs, and the trends in θ_{AT} and θ_{GC} are well reproduced by the model (Figure 7a–d). Even at the lowest temperature

DOI: 10.1021/jacs.6b05854
J. Am. Chem. Soc. 2016, 138, 11792–11801

sampled, ~5 °C, only ~90% of the population is fully duplexed for both the GC-core and GC-mix sequences. The shape of the frayed dimer distribution indicates that, as the temperature increases, a few initial base pair contacts break leading to partially melted stable configurations, the population of which accumulates gradually and peaks ~10 °C below T_m. But as the temperature increases past T_m, the ensemble of fully intact dimer and partially melted dimer states quickly drops off coincident with a sharp rise in the monomer population.

The population profile for the AT-all sequence predicts a comparatively small frayed dimer population, with 85% accounted for by states with only a single broken base pair. Moreover, microstates with 9 AT base pairs and the fully intact duplex of 10 AT base pairs would yield similar IR spectra, shedding additional light on the difficulty of resolving a distinct spectroscopic component for partially melted configurations for this sequence using the maximum entropy method (Figure 5h).

The lattice model also offers an opportunity to ask whether the frayed configurations, heterogeneous melting, and bimodal kinetics truly reflect transitions involving more than two thermodynamic states separated by barriers $>k_BT$. To test this, we used the lattice model to calculate a free energy landscape as a function of the number of intact base pairs for each oligonucleotide (n_{bp}) from the temperature-dependent probability distribution as $\Delta G(n_{bp}) = -k_BT\ln[P(n_{bp})]$, where the monomer state is taken as the reference state. These surfaces are plotted for the temperature extremes, T_m, and temperatures 20 °C above and below T_m (Figure 8). Each sequence is

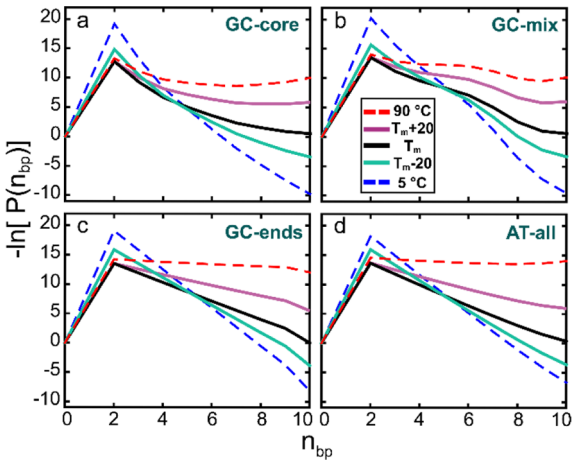

Figure 8. Free energy surfaces calculated using the lattice model for (a) GC-core, (b) GC-mix, (c) GC-ends, and (d) AT-all at 5 °C, T_m − 20 °C, T_m, T_m + 20 °C, and 90 °C.

predicted to have two stable minima separated by a barrier at n_{bp} = 2 at all temperatures, as expected for thermodynamically two-state melting. (Note this model does not consider n_{bp} = 1; see SI.) The primary differences between sequences are the shape and location of the dimer minimum on this landscape. Whereas the positions of the two minima are at n_{bp} = 0 and n_{bp} = 10 for GC-ends, the position of the minimum in the dimer basin shifts from n_{bp} = 10 to n_{bp} = 7 between 5 and 90 °C for GC-core. GC-mix appears to be the sequence closest to a three-basin energy landscape, with a high temperature shoulder at n_{bp} = 6. This sequence-dependent, two-minima structure of the free energy surfaces is consistent with the free energy surfaces measured directly by single-molecule force clamp experiments for hairpins containing alternating AT and GC blocks of base pairs.[51]

Although a previous report has suggested the feasibility of using the NN parameters to analyze hybridization kinetics,[52] interpreting dehybridization dynamics on the basis of a free energy surface calculated from the equilibrium description of the lattice model should be done with caution. However, it does raise the question of how one would observe biexponential kinetics in a thermodynamically two-state system. Taking GC-core as an example, we see from Figure 8a that our T-jump is far from perturbative, functionally reshaping the energy landscape along which the dissociating system evolves.[53] As a consequence, the fast time scale in the relaxation kinetics reflects re-equilibration within the dimer basin through rapid fraying of the termini, followed by full dissociation through an activated process. This result highlights an important distinction when defining what makes a system "two-state". Although we find that some sequences demonstrate a diversity of partially melted conformations near T_m as opposed to only monomers and fully paired duplexes connected through the all-or-nothing loss of base pairing assumed by the standard two-state description of oligonucleotide dehybridization, we do not find definitive evidence for stable intermediate states in the thermodynamic sense of a local minimum along the dissociation pathway. While such low-dimensional energy landscapes calculated from a simple model should be regarded as suggestive rather than definitive, the observed time scales for fraying and diffusion on the free energy surface are consistent with this picture. It is possible that the "paired" state at higher temperatures reflects many frayed configurations that exchange relatively rapidly on a 10−100 ns time scale, and that the full dissociation events are relatively rare events oberved on the 10−30 μs time scale. Further work will test the accuracy of this description by characterizing the relaxation kinetics for multiple initial and final temperatures.

The hybridization mechanism suggested by our results is consistent with the zippering mechanism derived from both experiment[9,10,14] and simulation[21,22] for heterogeneous sequences in which an initial critical nucleus of stable base pairs forms as the rate-limiting step followed by rapid "zippering" of the remaining base pairs into place. However, the fast response we assign to duplex fraying has not been analyzed in detail in these past experiments due to the limits on the time resolution of capacitive discharge T-jump techniques. Fraying has been studied in equimolar mixtures of A and U RNA oligonucleotides, but this report was restricted to temperatures below T_m due to the difficulty of isolating fraying from single strand destacking at higher temperatures.[54] Measuring the UV hyperchromicity reports primarily on the degree of global base stacking while IR experiments track the base-specific features necessary to distinguish which bases are invovled in pre-dissociation melting. We believe our results provide direct experimental confirmation of the zipper mechanism inferred from these early T-jump experiments as well as the sequence-directed zippering predicted in coarse-grained simulations of DNA hybridization.

CONCLUSION

The structural resolution afforded by linear and 2D IR spectroscopy along with the nanosecond to millisecond time resolution of T-jump IR experiments presents an effective strategy for studying the dissociation of DNA oligonucleotides in detail. Combining these data with a simple lattice model

DOI: 10.1021/jacs.6b05854
J. Am. Chem. Soc. 2016, 138, 11792−11801

allows explicit consideration of the microstates populated along the helix-to-coil transition. We have applied these methods to a model set of DNA 10-mers and find that the extent of deviation from the two-state assumption is dictated by the nucleobase sequence. Overall, the sequences tested can be arranged in order of increasing deviation from simple two-state behavior, GC-ends < AT-all < GC-mix < GC-core, where at either extreme GC-ends dissociates in an essentially all-or-nothing manner while GC-core passes through sizeable, partially melted populations along the transition. The observed temperature trends and kinetics follow naturally when weighing the interplay of base pairing, where AT base pairs are generally weaker than GC base pairs, against the entropic drive to dissociate the duplex.

Despite the contrast in the amount of populated partially melted configurations for each of the sequences, our data suggest that all of these self-complementary sequences dissociate along a similar dehybridization pathway, with the ends of the helix fraying first. The stability of these frayed dimers, and ultimately the degree of deviation from an all-or-nothing dissociation, is dictated by the nucleobase sequence, as is the nature of the frayed dimer configurations themselves. A combination of IR spectroscopies proves capable of resolving and characterizing stable partially melted configurations that give rise to heterogeneity in the folded ensemble, as well as tracking and identifying base-specific features of the dissociation mechanism on a nanosecond to millisecond time scale, and ultimately provides an experimentally consistent and non-invasive means to address the DNA dehybridization mechanism in detail beyond a simple two-state picture. We believe the strategy presented here will prove generally applicable to the detailed characterization of folding and hybridization in nucleic acid systems.

MATERIALS AND METHODS

Oligonucleotide Samples. All DNA samples were purchased from Integrated DNA Technologies (IDT) at desalt-grade purity. Oligonucleotides were further purified using centrifugal membrane filters with a 3 kDa cutoff. Labile protons were HD exchanged in deuterated water (D_2O, Cambridge Isotopes). All DNA samples were prepared at a concentration of 2 mM in deuterated sodium phosphate buffer (pD 7.2) with 240 mM NaCl and 18 mM $MgCl_2$. These buffer conditions were selected such that the T_m of the oligonucleotides would fall around 50 °C, since this is the middle of the accessible temperature range for a D_2O solvent. The samples were dissolved in D_2O in preparation for IR spectroscopy to remove the interference from the H_2O bend absorption at 1650 cm^{-1}. The oligonucleotide concentration was checked on a NanoDrop UV/vis spectrometer (Thermo Scientific) to within ±0.5 mg/mL. Samples were annealed by heating to 95 °C and then cooling gradually to room temperature over 10−15 min.

Temperature Ramp FTIR. For all IR spectroscopy, samples were held between two CaF_2 windows with a 50 μm Teflon spacer defining the path length and mounted in a home-built brass sample cell connected to a recirculating chiller to control the sample temperature. The bath temperature was ramped between 0 and 96 °C in 3 °C steps, and the temperature at the sample was recorded with a thermocouple embedded in the brass sample jacket, resulting in a range of ∼5−90 °C. Spectra were recorded on a Bruker Tensor 27 FTIR spectrometer at 4 cm^{-1} resolution, averaging 30 scans at each temperature step after waiting 60 s for the sample cell to equilibrate at each bath set point.

Temperature Ramp 2D IR. The sample assembly for temperature ramp 2D IR was identical to the FTIR assembly above. For 2D IR spectroscopy, the bath temperature was ramped between 10 and 90 °C in 10 °C steps, resulting in a sample temperature range of ∼13−83 °C. 2D IR spectra were acquired using a spectrometer built to a previously desribed design.[55] The polarization was set to perpendicular (ZZYY), the waiting time was fixed at τ_2 = 150 fs, and the evolution time τ_1 was scanned out to 3.0 ps in 4 fs steps.

t-HDVE Spectroscopy. The starting temperature for each of the sequences was selected such that the temperature was jumped 18 °C cross the center of the frayed dimer population distribution: GC-core ,43 °C; GC-mix, 43 °C; GC-ends, 35 °C; and AT-all, 29 °C. The temperature jump spectrometer has been described previously.[44] The t-HDVE spectra were collected using the Fourier transform spectral interferometry method,[45] with the local oscillator stepped from −10 to 10 fs in 5 fs steps. The polarization was set to ZZZZ. Time traces represent at least 10 averaged data sets.

ASSOCIATED CONTENT

Supporting Information

The Supporting Information is available free of charge on the ACS Publications website at DOI: 10.1021/jacs.6b05854.

Details of the lattice model; thermodynamic analysis of melting curves; maximum entropy reconstruction; temperature ramp 2D IR series; SVD components for the GC and AT cross peak regions; contact plots calculated from the lattice model; GC kinetic traces from t-HDVE (PDF)

AUTHOR INFORMATION

Corresponding Author

*tokmakoff@uchicago.edu

Notes

The authors declare no competing financial interest.

ACKNOWLEDGMENTS

We thank the National Science Foundation (Grant Nos. CHE-1414486 and CHE-1561888) for support of this research.

REFERENCES

(1) Bell, S. P.; Dutta, A. *Annu. Rev. Biochem.* **2002**, *71*, 333.
(2) Kunkel, T. A.; Bebenek, K. *Annu. Rev. Biochem.* **2000**, *69*, 497.
(3) Mandal, M.; Breaker, R. R. *Nat. Rev. Mol. Cell Biol.* **2004**, *5*, 451.
(4) Sherwood, A. V.; Henkin, T. M. *Annu. Rev. Microbiol.* **2016**, 70.
(5) Schulze, A.; Downward, J. *Nat. Cell Biol.* **2001**, *3*, E190.
(6) Lin, X.; Sun, X.; Luo, S.; Liu, B.; Yang, C. *TrAC, Trends Anal. Chem.* **2016**, *80*, 132.
(7) Seeman, N. C. *Trends Biochem. Sci.* **2005**, *30*, 119.
(8) Seeman, N. C. *Mol. Biotechnol.* **2007**, *37*, 246.
(9) Wetmur, J. G.; Davidson, N. *J. Mol. Biol.* **1968**, *31*, 349.
(10) Pörschke, D.; Eigen, M. *J. Mol. Biol.* **1971**, *62*, 361.
(11) Mergny, J.-L.; Lacroix, L. *Oligonucleotides* **2003**, *13*, 515.
(12) Marky, L. A.; Breslauer, K. J. *Biopolymers* **1987**, *26*, 1601.
(13) SantaLucia, J. *Proc. Natl. Acad. Sci. U. S. A.* **1998**, *95*, 1460.
(14) Pörschke, D.; Uhlenbeck, O.; Martin, F. *Biopolymers* **1973**, *12*, 1313.
(15) Owczarzy, R.; Moreira, B. G.; You, Y.; Behlke, M. A.; Walder, J. A. *Biochemistry* **2008**, *47*, 5336.
(16) Hagan, M. F.; Dinner, A. R.; Chandler, D.; Chakraborty, A. K. *Proc. Natl. Acad. Sci. U. S. A.* **2003**, *100*, 13922.
(17) Maffeo, C.; Yoo, J.; Comer, J.; Wells, D.; Luan, B.; Aksimentiev, A. *J. Phys.: Condens. Matter* **2014**, *26*, 413101.
(18) Mentes, A.; Florescu, A. M.; Brunk, E.; Wereszczynski, J.; Joyeux, M.; Andricioaei, I. *Biophys. J.* **2015**, *108*, 1727.
(19) Ouldridge, T. E.; Louis, A. A.; Doye, J. P. *J. Chem. Phys.* **2011**, *134*, 085101.
(20) Hinckley, D. M.; Freeman, G. S.; Whitmer, J. K.; de Pablo, J. J. *J. Chem. Phys.* **2013**, *139*, 144903.
(21) Ouldridge, T. E.; Šulc, P.; Romano, F.; Doye, J. P.; Louis, A. A. *Nucleic Acids Res.* **2013**, *41*, 8886.

DOI: 10.1021/jacs.6b05854
J. Am. Chem. Soc. 2016, 138, 11792−11801

(22) Hinckley, D. M.; Lequieu, J. P.; de Pablo, J. J. *J. Chem. Phys.* **2014**, *141*, 035102.
(23) Ma, H.; Proctor, D. J.; Kierzek, E.; Kierzek, R.; Bevilacqua, P. C.; Gruebele, M. *J. Am. Chem. Soc.* **2006**, *128*, 1523.
(24) Chen, C.; Wang, W.; Wang, Z.; Wei, F.; Zhao, X. S. *Nucleic Acids Res.* **2007**, *35*, 2875.
(25) Ma, H.; Wan, C.; Wu, A.; Zewail, A. H. *Proc. Natl. Acad. Sci. U. S. A.* **2007**, *104*, 712.
(26) Morrison, L. E.; Stols, L. M. *Biochemistry* **1993**, *32*, 3095.
(27) Rauzan, B.; McMichael, E.; Cave, R.; Sevcik, L. R.; Ostrosky, K.; Whitman, E.; Stegemann, R.; Sinclair, A. L.; Serra, M. J.; Deckert, A. A. *Biochemistry* **2013**, *52*, 765.
(28) SantaLucia, J.; Allawi, H. T.; Seneviratne, P. A. *Biochemistry* **1996**, *35*, 3555.
(29) Breslauer, K. J.; Frank, R.; Blöcker, H.; Marky, L. A. *Proc. Natl. Acad. Sci. U. S. A.* **1986**, *83*, 3746.
(30) Patel, D. J.; Hilbers, C. *Biochemistry* **1975**, *14*, 2651.
(31) Breslauer, K. J.; Sturtevant, J. M.; Tinoco, I. *J. Mol. Biol.* **1975**, *99*, 549.
(32) Yin, Y.; Zhao, X. S. *Acc. Chem. Res.* **2011**, *44*, 1172.
(33) Nonin, S.; Leroy, J.-L.; Gueron, M. *Biochemistry* **1995**, *34*, 10652.
(34) Brauns, E. B.; Dyer, R. B. *Biophys. J.* **2005**, *89*, 3523.
(35) Stancik, A. L.; Brauns, E. B. *Biochemistry* **2008**, *47*, 10834.
(36) Narayanan, R.; Zhu, L.; Velmurugu, Y.; Roca, J.; Kuznetsov, S. V.; Prehna, G.; Lapidus, L. J.; Ansari, A. *J. Am. Chem. Soc.* **2012**, *134*, 18952.
(37) Peng, C. S.; Jones, K. C.; Tokmakoff, A. *J. Am. Chem. Soc.* **2011**, *133*, 15650.
(38) Banyay, M.; Sarkar, M.; Gräslund, A. *Biophys. Chem.* **2003**, *104*, 477.
(39) Marmur, J.; Doty, P. *J. Mol. Biol.* **1962**, *5*, 109.
(40) Krummel, A. T.; Zanni, M. T. *J. Phys. Chem. B* **2006**, *110*, 13991.
(41) Dai, Q.; Sanstead, P. J.; Peng, C. S.; Han, D.; He, C.; Tokmakoff, A. *ACS Chem. Biol.* **2016**, *11*, 470.
(42) Lumry, R.; Biltonen, R.; Brandts, J. F. *Biopolymers* **1966**, *4*, 917.
(43) Widjaja, E.; Garland, M. *J. Comput. Chem.* **2002**, *23*, 911.
(44) Chung, H. S.; Khalil, M.; Smith, A. W.; Tokmakoff, A. *Rev. Sci. Instrum.* **2007**, *78*, 063101.
(45) Jones, K. C.; Ganim, Z.; Peng, C. S.; Tokmakoff, A. *J. Opt. Soc. Am. B* **2012**, *29*, 118.
(46) Chen, S.-J.; Dill, K. A. *Proc. Natl. Acad. Sci. U. S. A.* **2000**, *97*, 646.
(47) Everaers, R.; Kumar, S.; Simm, C. *Phys. Rev. E* **2007**, *75*, 041918.
(48) Zimm, B. H. *J. Chem. Phys.* **1960**, *33*, 1349.
(49) Applequist, J.; Damle, V. *J. Am. Chem. Soc.* **1965**, *87*, 1450.
(50) Zeng, Y.; Montrichok, A.; Zocchi, G. *J. Mol. Biol.* **2004**, *339*, 67.
(51) Woodside, M. T.; Anthony, P. C.; Behnke-Parks, W. M.; Larizadeh, K.; Herschlag, D.; Block, S. M. *Science* **2006**, *314*, 1001.
(52) Ohmichi, T.; Nakamuta, H.; Yasuda, K.; Sugimoto, N. *J. Am. Chem. Soc.* **2000**, *122*, 11286.
(53) Chung, H. S.; Shandiz, A.; Sosnick, T. R.; Tokmakoff, A. *Biochemistry* **2008**, *47*, 13870.
(54) Pörschke, D. *Biophys. Chem.* **1974**, *2*, 97.
(55) DeFlores, L. P.; Nicodemus, R. A.; Tokmakoff, A. *Opt. Lett.* **2007**, *32*, 2966.

DOI: 10.1021/jacs.6b05854
J. Am. Chem. Soc. 2016, 138, 11792−11801